Precision Agriculture, 5, 275–289, 2004


# Spider Mite Detection and Canopy Component Mapping in Cotton Using Hyperspectral Imagery and Spectral Mixture Analysis

GLENN J. FITZGERALD gfitzgerald@uswcl.ars.ag.gov
*USDA-ARS, U.S. Water Conservation Laboratory, Phoenix, AZ 85040*

STEPHAN J. MAAS
*Department Plant & Soil Science, Texas Tech University, 3810 4th St., Lubbock, TX 79415*

WILLIAM R. DETAR
*USDA-ARS, Western Integrated Cropping Systems Research Center, Shafter, CA 93263*

**Abstract.** Spectral mixture analysis and hyperspectral remote sensing are analytical and hardware tools new to precision agriculture. They can allow detection and identification of various crop stresses and other plant and canopy characteristics through analysis of their spectral signatures. One stressor in cotton, the strawberry spider mite (*Tetranychus turkestani U.N.)*, feeds on plants causing leaf puckering and reddish discoloration in early stages of infestation and leaf drop later. To determine the feasibility of detecting the damage caused by this pest at the field level, AVIRIS imagery was collected from USDA-ARS cotton research fields at Shafter, CA on 4 dates in 1999. Additionally, cotton plants and soil were imaged *in situ* in 10 nm increments from 450 to 1050 nm with a liquid-crystal tunable-filter camera system. Mite-damaged areas on leaves, healthy leaves, tilled shaded soil, and tilled sunlit soil were chosen as reference endmembers and used in a constrained linear spectral mixture analysis to unmix the AVIRIS data producing fractional abundance maps. The procedure successfully distinguished between adjacent mite-free and mite-infested cotton fields although shading due to sun angle differences between dates was a complicating factor. The resulting healthy plant, soil, mite-damaged, and shade fraction maps showed the distribution and relative abundance of these endmembers in the fields. These hardware and software technologies can identify the position, spatial extent, and severity of crop stresses for use in precision agriculture.

**Keywords:** spider mite, hyperspectral, remote sensing, spectral mixture analysis, pest detection, cotton

## Introduction

The strawberry spider mite causes serious damage to cotton in the San Joaquin Valley in California. They feed on plants, causing leaf puckering and reddish discoloration in early stages of infestation and leaf drop later (Anonymous, 1996). Because of these leaf-color changes, and perhaps physiological changes not visible to the naked eye, remote sensing and image processing offer the possibility of identifying regions within fields that indicate spider mite damage. Typically, mite control is achieved by spraying the entire field with pesticides after field scouting has identified a threshold number of individuals. However, if infested areas in a field can be

identified, pesticide applications could be targeted, reducing input costs and benefiting the environment through reduction of applied pesticides.

Remote sensing represents one method for mapping the spatial distribution and severity of anomalies, including damage caused by spider mites. Multispectral remote sensing has been shown to be effective at relating reflectance to the incidence of agronomic pests, including disease (Summy *et al*., 1997), weeds (Brown *et al*., 1994), and mites (Fitzgerald *et al*., 1999a, 1999b; Peñuelas *et al*., 1995;) but due to limited spectral coverage, multispectral remote sensing may not be able to uniquely identify the damage-causing stressor. Hyperspectral remotely sensed data provide dozens to hundreds of contiguous narrow spectral bands, forming spectral curves of the scene components of interest. Analysis of the shapes of these spectra allow discrimination of the scene components. The large amount of data in hyperspectral imagery permits the application of advanced image analysis techniques designed to extract unique data features from high-dimensional data sets and reduce complexity to make the data more interpretable. One technique, spectral mixture analysis (SMA), was used in this paper because it allows identification and quantification of scene components of interest, is relatively simple conceptually, is not computationally intensive, and is readily available as part of commercial software packages.

Spectral mixture analysis has been used to process imagery from ecological and landscape studies for a number of years and the details of the procedure are well documented beginning with Adams and Smith (1986) and more recently in Okin *et al*. (2001). One type of SMA, linear spectral unmixing, is based on the assumption that each pixel is a physical mixture of multiple components (endmembers) and the spectrum of this mixed pixel is a linear combination of the endmember reflectance spectra (Tompkins *et al.,* 1997). SMA also assumes that a small number of spectra representing the endmembers can describe most of the spectral variation in a scene and be used to ''unmix'' the pixels and determine the relative fractional abundance of each endmember on a per-pixel basis. This approach could allow discrimination of one plant stress from another through identification of unique spectral absorption features or differences in the shapes of the spectral curves and quantify the amount present in each pixel. Thus, the fractional abundance maps produced can indicate both the spatial extent and severity of particular stresses. Abundance maps would permit a farm manager or scout to locate precisely the identified stress in a field, thereby providing for guided field scouting and precision application of appropriate control measures such as pesticides or biological control agents.

Few papers have addressed the issue of detection or discrimination of canopy-level features in agricultural crops with hyperspectral remote sensing (Estep and Davis, 2001; Gat *et al*., 1999; Gat *et al*., 2000; Green *et al*., 1998; Perry *et al*., 2000). A few published papers have discussed field-scale soil properties (Palacios-Orueta and Ustin, 1996; Whiting and Ustin, 2001). Some studies have addressed leaf-scale measurements in agricultural crops and forests and others have measured single-plant scale spectra and associated biophysical characteristics. Examples include relating leaf reflectance to leaf water status (Bowman, 1989; Carter, 1991; Hunt and Rock, 1989; Tian *et al*., 2001), changes in the red-edge due to stress conditions (Curran *et al*., 1990; Railyan and Korobov, 1993), and imposition of various nutrient-deficiency stresses (Masoni *et al*., 1996). Carter and Knapp (2001) reviewed

the effects of various physical and biological stressors on the reflectance of various species of leaves, mostly from trees.

The principal objective of this research was to determine whether hyperspectral imagery that had been "unmixed" could accurately discriminate between a field of healthy cotton and an adjacent field of mite-damaged cotton based on reference endmembers in a spectral library collected from the field plots. Additionally, it was expected that the SMA procedure would provide abundance fraction images delivering spatially explicit maps of mite damage severity useful within the framework of precision agriculture.

## Materials and methods

An experiment was established on two, 2.8 ha fields at the USDA-ARS research station in Shafter, CA (35.5°N, 119.3°W, 120 m above sea level). Each field (Figure 1) was planted to cotton (*Gossypium hirsutum* L. variety "Maxxa") on May 4, 1999 (DOY 124). Both fields were irrigated with sub-surface drip irrigation, which left the soil surface dry all season. Both were managed according to standard cultural practices for cotton in the area except that one (Field 41) was sprayed once with a wide spectrum pesticide about eight weeks after planting, virtually eliminating beneficial insects and predatory mites, which normally keep spider mite populations in check. The other (Field 42) was treated with appropriate pesticides several times during the growing season to control spider mite infestations following standard local practices.

Each field was divided into 20 sections for mite population counting, which was performed weekly to monitor spatial and temporal distribution of the mites in each field. Using published guidelines (Anonymous, 1996), 10 leaves within each section were examined for presence or absence of mites. Normally, such a count would be

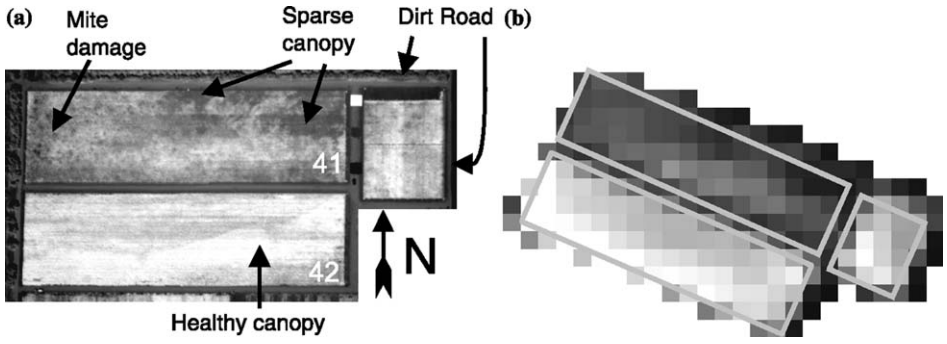


*Figure 1.* (a) High resolution (0.65 m) near-infrared image (850 nm) of cotton research Fields 41 and 42 acquired on 25 Aug 1999. In Field 41, mites were allowed to damage the crop while in Field 42 mites were controlled. Arrows point to scene features. Fields 41 and 42 each had dimensions of approximately 100 m × 300 m. The smaller field to the right of Fields 41 and 42 was not part of this experiment but is shown so that the surrounding roads could be included in the analysis. (b) AVIRIS image (band 41, 845 nm, 18 m pixel resolution) of the same fields acquired 28 Aug 1999.

made for an entire field, but each section was tallied in order to gain an understanding of the spatial distribution of the mites within the two fields.

A digital camera system consisting of visible and near-infrared "Varispec" liquid-crystal tunable-filters (LCTF) from Cambridge Research Instrumentation, Inc., Woburn, MA, USA and a digital camera from PixelVision, Inc., Tigard, OR, USA (Pluto model, 14-bit, cooled, 512 × 512 pixels) was mounted aboard a platform with the operator on a high-clearance vehicle capable of entering cotton fields. The liquid-crystal filters were tuned electronically at 9.5 nm increments from 400 to 1050 nm allowing narrow-band wavelengths of light to reach the camera. The camera shutter and filter were synchronized so that one image was acquired for each waveband. Each image set was acquired in less than 3 min, within 1 h of solar noon, and stored digitally on a laptop computer. At a height of about 3 m above the canopy, pixel resolution was about 1 mm. Scene components included healthy leaves, mite-infested leaves, sunlit soil, open cotton boll, dead leaves, and canopy shade. Images were corrected to reflectance using a 99% "Spectralon" calibration panel (Labsphere, North Sutton, NH, USA), which was placed in the field of view before and after image acquisition.

Imagery from NASA's Airborne Visible Infrared Imaging Spectrometer (AVIRIS) was acquired for the research fields on four separate dates in 1999. Flight dates, day of year (DOY), local times, and solar zenith angle are shown in Table 1. The hyperspectral data from AVIRIS was composed of 224 images acquired contiguously from 400 to 2500 nm in 10 nmbands. The AVIRIS data sets were atmospherically corrected and converted to reflectance using ATREM and EFFORT algorithms. Ground pixel resolution was 18 m.

Images acquired from the LCTF system were used to build a spectral library containing representative endmembers, including sunlit healthy leaves (H), sunlit mite-damaged leaves (M), tilled sunlit soil (S), tilled shaded soil (Sh), opened cotton boll (CB), and dead leaf (D) (Figure 2). Other spectra in the library not shown here included leaf shade on dry soil (LSS), leaf shaded by leaves (LSL), and sunlit soil within the canopy (SSC). Reference spectra were constructed by selecting representative pixels on leaves and soil. The number of pixels selected from the areas to create each endmember spectrum was: H, 900; M,16; S, 5000; Sh, 100; CB, 9; and D, 27. The SSC and LSS spectra collected within the canopy showed a red edge effect due to the scatter of light from the surrounding leaves, so S and Sh were selected from a separate LCTF image cube of tilled soil located outside the plant canopy. This gave a "purer" shade component without mixing with plant spectral features.

*Table 1.* AVIRIS overflight dates, day of year (DOY), local times (Pacific Daylight Time), and solar zenith angles

| Flight date | DOY | Local time | Solar zenith |
|---|---|---|---|
| 13 Jun 1999 | 164 | 11:29 am | 22.7° |
| 28 Aug 1999 | 240 | 12.09 pm | 27.9° |
| 1 Sep 1999 | 244 | 10:07 am | 49.3° |
| 24 Sep 1999 | 267 | 11:43 am | 38.9° |

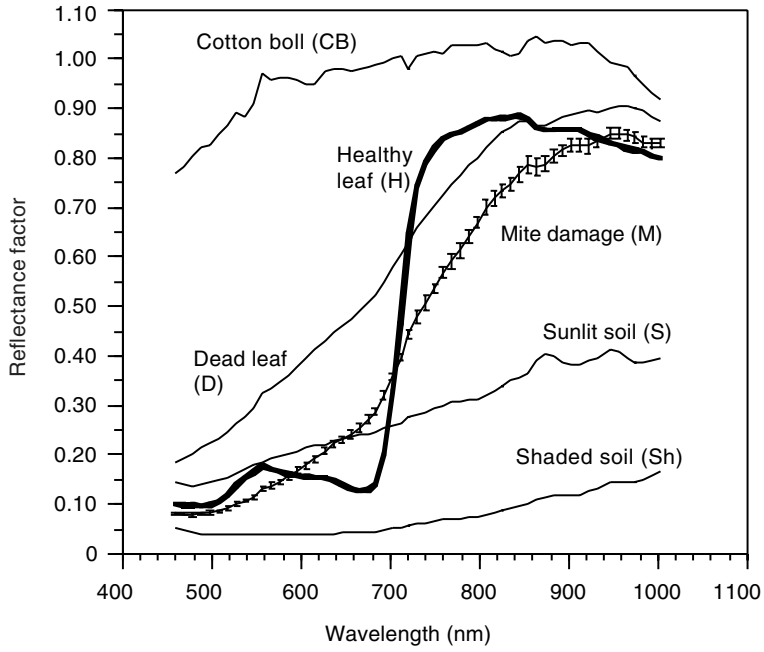


*Figure 2.* Six spectral library endmembers derived from scene components in the ground-based liquid-crystal tunable-filter camera imagery. The error bars represent ± 1 standard error. These are shown for the mite-damage curve only because standard errors for the other curves were too small to show clearly.

This ground-based approach allowed selection of more spectrally "pure" or non-mixed endmember spectra than could be selected from the mixed pixels in the AVIRIS imagery (Gillespie *et al.*, 1990). Selection of the "purest" or representative endmember spectra is a requirement for proper spectral unmixing since these spectra are used as references to derive fractional abundances.

The AVIRIS image cubes were masked to include only the fields of interest and then spectrally resampled to match the wavelengths of the more restricted LCTF spectral library after noisy bands below about 450 nm and above 1000 nm were removed. This spectral resampling yielded a total of 57 wavebands in 9.5 nm increments from 459 to 1002 nm. Spectral mixture analysis was then performed on the four AVIRIS images using the built-in linear spectral unmixing routine in the ENVI software package (Research Systems, Inc., Boulder, CO). Within ENVI, analysis parameters were set to constrained unmixing with a weight of 10, which constrained the fractions within each pixel to sum to unity.

The abundance fractions represent the relative area occupied by an endmember within a pixel. To have realistic values they need to fall between 0 and 1 and the totals sum to unity. If the resulting fractions are highly negative or much greater than unity then the number and type of endmembers were not chosen properly. Values slightly negative or greater than unity are allowed to account for noise in the data. Pixels should have a low RMSE near the magnitude of instrument noise

(Anonymous, 2000; Roberts *et al.,* 1998; Smith *et al.,* 1990), typically below 0.025.

One feature of simple mixture modeling is that it assumes the same set of endmembers are present in all pixels, which is not reasonable since the composition of scene components will vary across an image. For example, a pixel can contain a mixture of canopy and shade or canopy, mite-damaged leaves, and shade. To vary the number and type of endmembers on a per-pixel basis, a simplified version of the multiple endmember spectral mixture analysis (MESMA) routine presented by Roberts *et al.* (1998) was utilized to assign the proper number and types of endmembers to each pixel. The criteria for this MESMA analysis were: Acceptable fraction abundances were set to range from −0.01 to 1.01, RMSE with no constraints (all RMSE values valid), and there was no residual criterion since this has not been shown to be a significant selector for endmembers (D.A. Roberts, pers. comm., 2002). Roberts *et al.* (1998) selected final pixel endmember combinations from 2 to 3 endmember models. This present study included 2–4 endmember models for each pixel. If more than one model met the selection criteria for any pixel, the one with the lowest RMSE was selected as the final model.

The MESMA model uses a large library of hundreds of endmembers and the selection of realistic combinations of endmembers for each pixel includes optimization of model selection, reduction of the number of potential models from hundreds to dozens, and an assessment of spatial context for the models (Roberts *et al.*, 1998). In this study, each pixel was modeled from a library of only nine endmembers: H, M, S, Sh, LSS, LSL, SSC, D, and CB. Restriction of the pool of potential endmembers greatly decreased the complexity of the modeling process. The danger is that not all endmembers present in the scene will be found in the library but given *a priori* knowledge of the field this possibility can be reduced or eliminated. Note that the abundance fractions of the final selected endmember sets summed to between 0.99 and 1.0 and the MESMA routine was constrained to include Sh in each pixel, reducing the number of possible endmember combinations and further simplifying the procedure.

The linear mixture model takes the form, Eq. (1):

$$P'_{i\lambda} = \sum_{k=1}^{N} \not f_{ki} * P_{k\lambda} + \varepsilon_{i\lambda} \quad \text{and} \quad \sum_{k=1}^{N} \not f_{ki} = 1, \tag{1}$$

where $P'_{i\lambda}$ is the spectral mixture at location $i$ modeled as the sum of $N$ reference endmembers, $P_{k\lambda}$, with each weighted by the fraction, $\not f_{ki}$. The unmodeled portion is the residual term, $\varepsilon_{i\lambda}$ at wavelength $\lambda$ and the endmember fractions were constrained to sum to 1. The error associated with the model fit was assessed through the root mean square error (RMSE), Eq. (2):

$$\text{RMSE}\left(\sum_{k=1}^{\lambda} (\varepsilon_{i\lambda})^2 \Big/ N\right)^{1/2}. \tag{2}$$

Yield monitor data were collected using an Agriplan 600 cotton yield monitor (Stow, MA, USA) with a Rockwell GPS unit and CSI differential receiver and are presented here as a surrogate for mite damage (discussed below). The yield data

were imported to the ENVI software to create an image map, masked, resampled, and registered to the AVIRIS data to permit pixel to pixel comparisons for regression analysis.

## Results

High resolution, near-infrared imagery collected with a multispectral system (Fitzgerald *et al.,* 1999b) showed a dark mite-damaged canopy in Field 41 while the vigorous canopy in Field 42 was bright (Figure 1(a)). Because more energy is reflected from healthy than unhealthy plants in the near-infrared, Field 42 appeared brighter than Field 41. Although ground pixel size was 18 m for the AVIRIS images (Figure 1(b)), there were noticeable light and dark patterns within each field, corresponding to those seen in Figure 1(a).

The two fields were managed identically except for mite control and the only other factor that could have differentially influenced the fields was soil variation. To test whether soil was a factor contributing to yield, the AVIRIS imagery from 13 Jun was selected to represent soil reflectance. This imagery was acquired 40 days after planting and ground cover was below 10%, thus it predominantly represented soil variation. Neither a regression of NDVI derived from the AVIRIS data from 13 Jun versus yield (not shown) nor S fraction from 13 Jun versus yield showed any relationships ($r^2 = 0$). Thus, soil was not a major factor in determining yield in these fields and it was determined the yield map could be used as a spatially explicit surrogate for mite damage severity. Yields in Fields 41 and 42 were 1338 and 3310 kg/ha, respectively. A *t*-test showed these were significantly different at $\alpha = 0.05$ ($P < 0.0001$).

The fields were statistically significantly different in terms of mite counts (Field 41 = 4.9 and Field 42 = 3.1 mites/10 leaves) as determined by a *t*-test at $\alpha = 0.05$ ($P = 0.0002$). Figure 3 shows yield versus mean mite counts for 21 Jul and 27 Jul. The $r^2$ value was 0.49 and the figure shows that mite populations at that time had a strong effect on final yield.

Five of the nine endmembers included in the spectral library were not selected in the final unmixed images (CB, D, LSL, LSS, SSC) either because they resulted in negative fractions or a few pixels met the criteria but these were located along field edges and mean fractions were less than 0.01. The combination of endmembers that consistently had the lowest RMSE, summed to unity, and correctly located known areas of mite-damaged plants, healthy plants, and soil was the combination that included S, M, H, and Sh, except for the 13 Jun image, which did not include M because mites were not present. Whenever Sh was excluded from the unmixing analysis, the sum of fractions ranged from 0.60 to 0.92. When Sh was included, all pixel abundances summed from 0.99 to 1.00.

Pixels forming Regions of Interest (ROI) were visually selected for Field 41 (mite-damaged), Field 42 (healthy canopy), and the dirt roads around the fields. Table 2a presents the numerical information for these regions and Figures 4 and 5 show the spatial distribution and intensity of these endmembers. To correct for

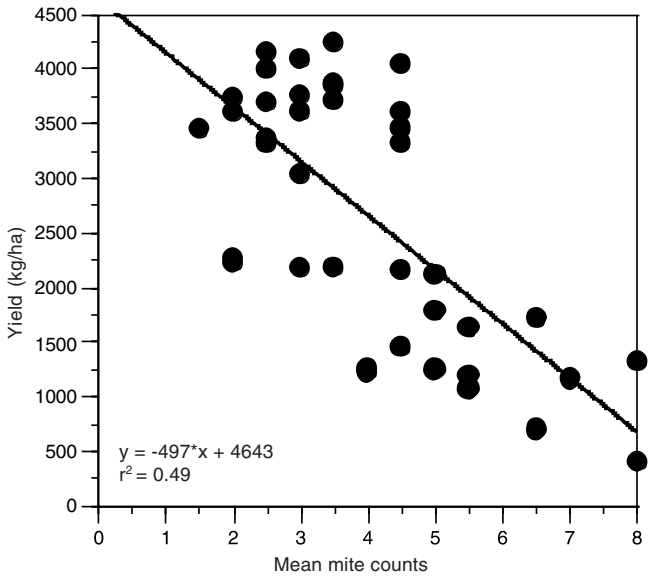


*Figure 3*. Yield as a function of mean mite counts from 21 Jul and 27 Jul for Fields 41 and 42. The yields above 3000 kg/ha are from Field 42 and the values below 3000 kg/ha are from Field 41.

shade, Eq. (3) was adapted from Adams *et al*. (1993) to normalize the effect of the shade fraction on M, H, and S fractions (Table 2b).

$$M_s = M/(1 - Sh), \tag{3}$$

where $M_s$ = mite fraction normalized for shade, $M$ = mite fraction, and Sh = shade fraction.

Equation (3) partly accounts for the effects of shaded leaves (Adams, *et al*., 1995) and improves comparisons of imagery acquired on different dates. Comparing $M$ fractions from 28 Aug and 1 Sep without shade normalization shows values of 0.09 and 0.01, respectively, a 9:1 ratio (Table 2a). With shade correction this changes to 0.20 and 0.04, respectively, a 5:1 ratio (Table 2b). Since these images were acquired only 4 days apart they would be expected to have similar fractions but these were confounded by shade (discussed below). Since shade is not a material component in an image, the fractions should be normalized for shade to give more accurate abundances (Tompkins *et al*., 1997).

The fraction images in Figure 4 show changes in the canopy throughout the season. On 13 Jun, 40 days after planting, ground cover in the fields was sparse as shown by the dark H pixels and brighter S pixels. Early season growth was most vigorous in the west side of the fields (Figures 4 and 5). Mean fractions on 13 Jun were almost identical as would be expected before mite pressures changed the growth characteristics of the two fields (Table 2a). Based on ground sampling in June, mean field mite counts were less than 1 mite per leaf and thus, the unmixing procedure correctly excluded the M endmember from the 13 Jun data.

*Table 2a.* Fractional abundance means, standard deviations, minimum, and maximum values by endmembers for Regions of Interest selected within Fields 41, 42, and the dirt roads surrounding the cotton fields

| | 13 Jun 99 | | | | 28 Aug 99 | | | | 1 Sep 99 | | | | 24 Sep 99 | | | |
|---|---|---|---|---|---|---|---|---|---|---|---|---|---|---|---|---|
| | Mean | SD | Min | Max | Mean | SD | Min | Max | Mean | SD | Min | Max | Mean | SD | Min | Max |
| Field 41 | | | | | | | | | | | | | | | | |
| Soil | 0.650 | 0.054 | 0.549 | 0.800 | 0.012 | 0.033 | 0 | 0.166 | 0 | 0 | 0 | 0 | 0.027 | 0.054 | 0 | 0.213 |
| Mite | 0 | 0 | 0 | 0 | 0.092 | 0.035 | 0.024 | 0.162 | 0.010 | 0.013 | 0 | 0.055 | 0.044 | 0.031 | 0 | 0.091 |
| Healthy | 0.043 | 0.016 | 0.010 | 0.080 | 0.344 | 0.058 | 0.247 | 0.472 | 0.240 | 0.027 | 0.188 | 0.309 | 0.280 | 0.096 | 0.154 | 0.519 |
| Shade | 0.307 | 0.041 | 0.182 | 0.381 | 0.552 | 0.033 | 0.461 | 0.626 | 0.750 | 0.025 | 0.691 | 0.805 | 0.649 | 0.062 | 0.481 | 0.725 |
| RMSE | 0.018 | 0.001 | 0.017 | 0.020 | 0.021 | 0.009 | 0.006 | 0.037 | 0.016 | 0.006 | 0.010 | 0.031 | 0.015 | 0.009 | 0.006 | 0.038 |
| Field 42 | | | | | | | | | | | | | | | | |
| Soil | 0.650 | 0.045 | 0.581 | 0.743 | 0 | 0 | 0 | 0 | 0 | 0 | 0 | 0 | 0 | 0 | 0 | 0 |
| Mite | 0 | 0 | 0 | 0 | 0 | 0 | 0 | 0 | 0 | 0 | 0 | 0 | 0.020 | 0.027 | 0 | 0.084 |
| Healthy | 0.046 | 0.011 | 0.018 | 0.062 | 0.630 | 0.049 | 0.558 | 0.765 | 0.400 | 0.037 | 0.332 | 0.480 | 0.401 | 0.100 | 0.237 | 0.597 |
| Shade | 0.304 | 0.034 | 0.234 | 0.365 | 0.370 | 0.049 | 0.234 | 0.441 | 0.600 | 0.037 | 0.519 | 0.668 | 0.579 | 0.082 | 0.402 | 0.690 |
| RMSE | 0.019 | 0.001 | 0.018 | 0.021 | 0.053 | 0.005 | 0.040 | 0.062 | 0.042 | 0.004 | 0.031 | 0.049 | 0.027 | 0.011 | 0.009 | 0.050 |
| Road | | | | | | | | | | | | | | | | |
| Soil | 0.882 | 0.081 | 0.750 | 0.974 | 0.715 | 0.075 | 0.582 | 0.832 | 0.464 | 0.126 | 0.345 | 0.775 | 0.576 | 0.105 | 0.467 | 0.782 |
| Mite | 0 | 0 | 0 | 0 | 0 | 0 | 0 | 0 | 0 | 0 | 0 | 0 | 0 | 0 | 0 | 0 |
| Healthy | 0 | 0 | 0 | 0 | 0.073 | 0.053 | 0 | 0.137 | 0.049 | 0.041 | 0 | 0.113 | 0.070 | 0.040 | 0 | 0.120 |
| Shade | 0.117 | 0.081 | 0.026 | 0.249 | 0.212 | 0.085 | 0.094 | 0.352 | 0.486 | 0.113 | 0.214 | 0.649 | 0.354 | 0.103 | 0.184 | 0.532 |
| RMSE | 0.027 | 0.004 | 0.022 | 0.034 | 0.018 | 0.005 | 0.013 | 0.029 | 0.019 | 0.003 | 0.015 | 0.024 | 0.015 | 0.004 | 0.010 | 0.023 |

Zero values indicate the absence of endmembers.

*Table 2b*. Fractional abundance means from Table 2a normalized for shade fraction

| | 13 Jun | 28 Aug | 1 Sep | 24 Sep |
|---|---|---|---|---|
| Field 41 | | | | |
| Soil | 0.938 | 0.027 | 0 | 0.077 |
| Mite | 0 | 0.205 | 0.040 | 0.125 |
| Healthy | 0.062 | 0.768 | 0.960 | 0.798 |
| Field 42 | | | | |
| Soil | 0.934 | 0 | 0 | 0 |
| Mite | 0 | 0 | 0 | 0.048 |
| Healthy | 0.066 | 1 | 1 | 0.952 |
| Road | | | | |
| Soil | 0.999 | 0.907 | 0.903 | 0.892 |
| Mite | 0 | 0 | 0 | 0 |
| Healthy | 0 | 0.093 | 0.095 | 0.108 |

The RMSE values are the same as those in Table 2a and are not repeated here.

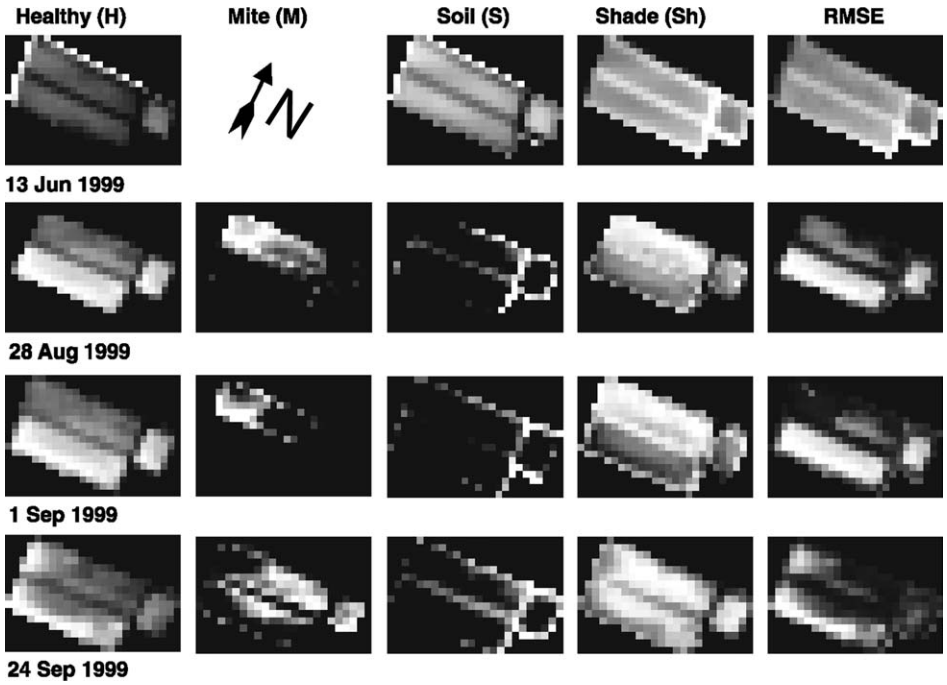


*Figure 4*. Fractional abundance image maps produced from spectral unmixing of four AVIRIS image cubes. Highest to lowest values are represented by brightest to darkest pixels. Black pixels have zero value. There was no abundance map for M on 13 Jun 1999 because all pixel values were zero.

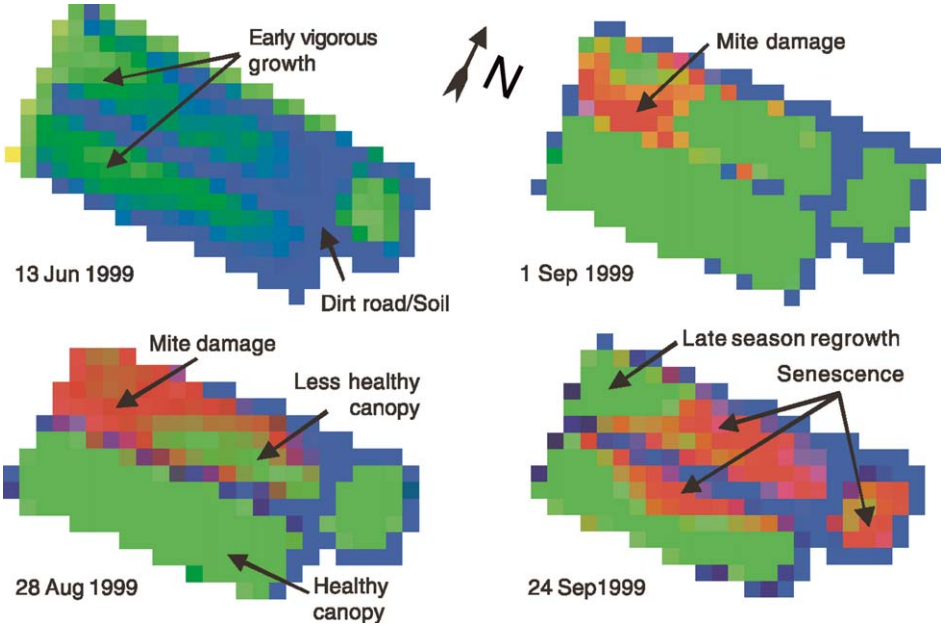


*Figure 5*. 3-band color composites normalized for shade of mite (red), healthy (green), and soil/road (blue) fraction images (from Figure 4). Red indicates mite-damaged areas that would assist a farmer or scout in locating them. Other ground features are indicated based on known conditions at the times of overflights.

The 28 Aug and 1 Sep images were acquired about six weeks after mite populations were first detected on the ground. Mite damage locations are evident and consistent for the two dates even though the shade-corrected mean fractions varied from 0.04 to 0.21 in Field 41 between the two dates (Table 2b). Importantly, the procedure did not generate false positives; no pixels with mite damage were identified in Field 42 for these dates. The S fraction was always greatest for the Road region and equal to zero in Field 42 once full canopy was established. The roads around the fields are clearly identified in Figures 4 and 5. The H abundances were greater for Field 42 than 41 for these dates.

By 24 Sep, a few weeks before harvest, senescence became a dominant feature. Some pixels are darker for H in Field 42 than the earlier dates (Figure 4) and the spatial patterns of bright pixels for the M images in Field 41 (Figure 4) and reddish pixels (Figure 5) changed from previous dates. When cotton senesces, it tends to form red spots on its leaves. The spectral signature from reddish senescent vegetation undoubtedly resembled that of M (Figure 2), although this was not measured. Late season regrowth of cotton is evident on the west side of Field 41 on 24 Sep by the bright pixels in the H image (Figure 4) and bright green pixels in Figure 5. This was noted on the ground as plants greater than 2 m tall.

Pixels in the Sh fraction images were brightest where there was more canopy variability along the edges of the fields and in the mite-infested and sparse canopy regions where there was a mix of canopy and soil (Figure 4). The mean Sh fractions

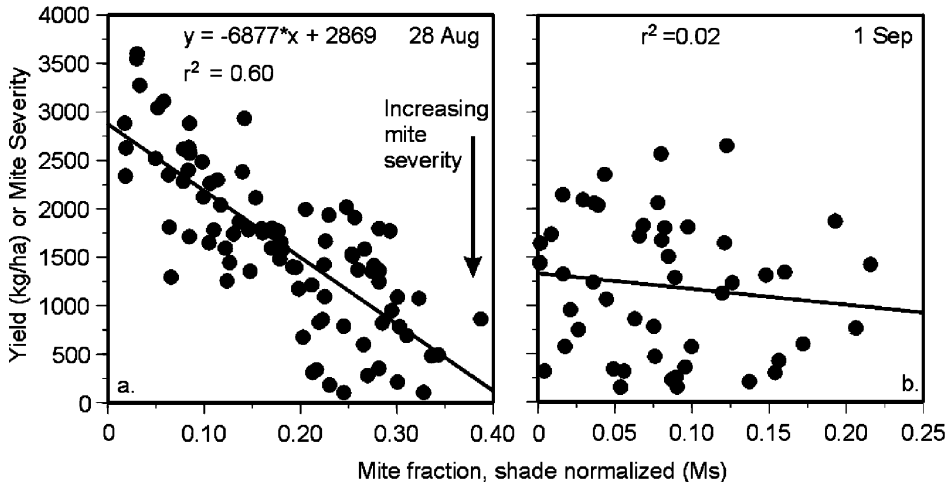


*Figure 6.* Pixel values from shade-normalized mite fractions ($M_s$) versus yield (or mite severity) registered to AVIRIS imagery. Yield monitor data were used as a surrogate for mite severity since this was the only factor influencing yield (see text). In (a), as mite fraction increased, the yield declined and mite severity increased. Figure 6b shows the same relationship but it is not statistically significant.

were always greatest in Field 41 and lowest in the Road ROI within a given date (Table 2a).

When $M_s$ from 28 Aug was plotted against yield (or mite severity) an $r^2$ of 0.60 was obtained (Figure 6(a)). There was no relationship when the same comparison was made for 1 Sep data ($r^2 = 0.02$).

## Discussion

Selecting a set of endmembers from a larger library based on selection criteria constraints such as having values between 0 and 1 and requiring all endmembers in a pixel to sum to unity provides a more realistic solution than assuming all pixels have the same endmembers. A few (2-4) endmembers are sufficient to describe the composition of each pixel and when selected from a larger library of endmembers can describe the variation across a scene. The result here was abundance images that matched known ground conditions. This procedure therefore incorporated both spectral and spatial variability. The comparison across four dates allowed a measure of temporal change to be incorporated into the analysis, which is critical for agriculture. The resulting images showed both consistent features and explainable changes in the crop (Figures 4 and 5), were able to distinguish between a mite-infested and mite-controlled field, and map the distribution and relative severity of mite damage.

Areas of severe mite damage were located consistently in the west (left) side of Field 41 on 28 Aug and 1 Sep, and Field 42 showed healthy canopy (Figures 4 and 5), which agrees with mite counts (Figure 3) and severity (Figure 6(a)).

However, because the solar zenith angles between dates were different, the abundance fractions were not the same (Table 2a) and the relation between mite severity and shade-corrected mite fraction ($M_s$) was basically non-existent on 1 Sep (Figure 6(b)). At best, mite-damaged leaves were less visible due to heavier shading on 1 Sep compared to 28 Aug and at worst, they were hidden underneath the upper canopy on 1 Sep. Sabol *et al.* (1992) noted that as shade fraction increases, the detection threshold for other endmembers is reduced. Despite the lack of a quantitative relationship of $M_s$ and mite severity for 1 Sep, the method was successful at a qualitative detection of damage in the same locations in Field 41 for both 28 Aug and 1 Sep (Figures 4 and 5). It appears that it can be difficult to compare abundance fractions across dates if the solar zenith angle is too great. This is likely due to nonlinear effects of plants shadowing plants (Roberts *et al.*, 1998).

Figure 5 integrates the fraction images in Figure 4 and corrects for shade effects. A map like this could be used as diagnostic tools for a farmer or scout either in a digital or paper form to locate mite damage. If loaded into a global-positioning-system-equipped handheld computer or downloaded into a tractor, this could guide personnel and machinery to the affected locations for appropriate treatment.

## Disclaimer and Acknowledgments

Mention of specific suppliers of hardware and software in this manuscript is for informative purposes only and does not imply endorsement by the United States Department of Agriculture. Thanks to Opto-Knowledge Systems, Inc. for calibrating AVIRIS data, supplying the liquid-crystal tunable-filter camera system, and technical support.

This research was supported, in part, through the NASA SSC Hyperspectral EOCAP project and a grant from Cotton, Incorporated. AVIRIS flights were provided by Jet Propulsion Laboratory, Pasadena, CA.

## References

Adams, J. B., Sabol, D. E., Kapos, V., Filho, R. A., Roberts, D. A., Smith, M. O. and Gillespie, A. R. 1995. Classification of multispectral images based on fractions of endmembers: Application to land-cover change in the Brazilian Amazon. Remote Sensing of Environment **52**, 137–154.

Adams, J. B. and Smith, M. O. 1986. Spectral mixture modeling: A new analysis of rock and soil types at the Viking Lander 1 Site. Journal Geophysical Research **91**, 8098–8112.

Adams, J. B., Smith, M. O. and Gillespie, A. R. 1993. Imaging spectroscopy: Interpretation based on spectral mixture analysis. In: *Remote Geochemical Analysis: Elemental and Mineralogical Composition*,Vol. 7, edited by C. M. Pieters and P. Englert (Cambridge University Press, NY, USA), pp. 145–166.

Anonymous 1996. *Integrated Pest Management for Cotton in the Western region of the United States*, 2nd ed (University of California, Division of Agriculture and Natural Resources), p. 164.

Anonymous 2000. *ENVI User's Guide* (Research Systems, Inc., Boulder, Colorado, USA), p. 930.

Bowman, W. D. 1989. The relationship between leaf water status, gas exchange, and spectral reflectance in cotton leaves. Remote Sensing of Environment **30**, 249–255.

Brown, R. B., Steckler, J.-P. G. A. and Anderson, G. W. 1994. Remote sensing for identification of weeds in no-till corn. Transactions of the ASAE **37**, 297–302.

Carter, G. A. 1991. Primary and secondary effects of water content on the spectral reflectance of leaves. American Journal of Botany **78**, 916–924.

Carter, G. A. and Knapp, A. K. 2001. Leaf optical properties in higher plants: Linking spectral characteristics to stress and chlorophyll concentration. American Journal of Botany **88**, 677–684.

Curran, P. J., Dungan, J. L. and Gholz, H. L. 1990. Exploring the relationship between reflectance red edge and chlorophyll content in slash pine. Tree Physiology **7**, 33–48.

Estep, L. and Davis, B. 2001. Nutrient stress detection in corn using neural networks and AVIRIS hyperspectral imagery. In: *Summaries of the 10th JPL Airborne Earth Science Workshop*, edited by R. O. Green (Jet Propulsion Laboratory, Pasadena, CA, USA), pp. 119–124.

Fitzgerald, G. J., Maas, S. J., and Detar, W. R. 1999a. Early detection of spider mites in cotton using multispectral remote sensing. In: *Proceedings of the Beltwide Cotton Conferences*, Orlando, FL, 3-7 Jan., edited by P. Dugger and D. A. Richter, (Natl. Cotton Council Am., Memphis, TN), pp. 1022–1024.

Fitzgerald, G. J., Maas, S. J., and Detar, W. R. 1999b. Detection of spider mites in cotton using multispectral remote sensing. In: *Proceedings of the 17th Biennial Workshop on Color Photography and Videography in Resource Assessment*, Reno, NV, 5–7 May, 1999, p. 77–82.

Gat, N., Erives, H., Fitzgerald, G. J., Kaffka, S. R. and Maas, S. J. 2000. Estimating sugar beet yield using AVIRIS-derived indices, In *Summaries of the 9th JPL Airborne Earth Science Workshop*, edited by R. O. Green (Jet Propulsion Laboratory, Pasadena, CA, USA), unpaginated CD.

Gat, N., Erives, H., Maas, S. J. and Fitzgerald, G. J. 1999. Application of low altitude AVIRIS imagery of agricultural fields I the San Joaquin Valley, CA to precision farming. In: *Summaries of the 8th JPL Airborne Earth Science Workshop*, edited by R. O. Green (Jet Propulsion Laboratory, Pasadena, CA, USA), pp. 145–150.

Gillespie, A. R., Smith, M. O., Adams, J. B., Willis, S. C., Fischer, A. F. and Sabol, D. E. 1990. Interpretation of residual images: Spectral mixture analysis of AVIRIS images, Owens Valley, California. In: *Summaries of the 2nd JPL Airborne Earth Science Workshop*, edited by R. O. Green (Jet Propulsion Laboratory, Pasadena, CA, USA), pp. 243–270.

Green, R. O., Pavri, B., Roberts, D. and Ustin, S. 1998. Mapping agricultural crops with AVIRIS spectra in Washington State. In: *Summaries of the 7th JPL Airborne Earth Science Workshop*, edited by R. O. Green (Jet Propulsion Laboratory, Pasadena, CA, USA), pp. 213–220.

Hunt, E. R. and Rock, B. N. 1989. Detection of changes in leaf water content using near- and middle-infrared reflectances. Remote Sensing of Environment **30**, 43–54.

Masoni, A., Ercoli, L. and Mariotti, M. 1996. Spectral properties of leaves deficient in iron, sulfur, magnesium, and manganese. Agronomy Journal **88**, 937–943.

Okin, G. S., Roberts, D. A., Murray, B. and Okin, W. J. 2001. Practical limits on hyperspectral vegetation discrimination in arid and semiarid environments. Remote Sensing of Environment **77**, 212–225.

Palacios-Orueta, A. and Ustin, S. 1996. Multivariate Statistical Classification of Soil Spectra. Remote Sensing of Environment **57**, 108–118.

Peñuelas, J., Filella, I., Lloret, P., Munoz, F. and Vilajeliu, M. 1995. Reflectance assessment of mite effects on apple trees. International Journal of Remote Sensing **16**, 2727–2733.

Perry, E. M., Gardner, M., Tagestad, J., Roberts, D., Cassady, P., Smith, J. and Nichols, D. 2000. Effects of image resolution and uncertainties on reflectance-derived crop stress indicators. In: *Summaries of the 9th JPL Airborne Earth Science Workshop*, edited by R. O. Green (Jet Propulsion Laboratory, Pasadena, CA, USA), unpaginated CD.

Railyan, V.Ya. and Korobov, R. M. 1993. Red edge structure of canopy reflectance spectra of triticale. Remote Sensing of Environment **46**, 173–182.

Roberts, D. A., Gardner, M., Church, R., Ustin, S., Scheer, G. and Green, R. O. 1998. Mapping Chaparral in the Santa Monica mountains using multiple endmember spectral mixture models. Remote Sensing of Environment **65**, 267–279.

Sabol, D. E., Adams, J. B. and Smith, M. O. 1992. Quantitative subpixel spectral detection of targets in multispectral images. Journal of Geophysical Research **97**, 2659–2672.

Smith, M. O., Ustin, S. L., Adams, J. B. and Gillespie, A. R. 1990. Vegetation in deserts: I. A regional measure of abundance from multispectral images. Remote Sensing of Environment **31**, 1–26.

Summy, K. R., Everitt, J. H., Escobar, D. E., Alaniz, M. A. and Davis, M. R. 1997. Use of airborne digital video imagery to monitor damage caused by two honeydew-excreting insects on cotton. In: *Proceedings of the 16th Biennial Workshop on Color Photography and Videography in Resource Assessment*, 29 Apr.–1 May, 1997, Weslaco, TX, pp. 238–244.

Tian, Q., Tong, Q., Pu, R., Guo, X. and Zhao, C. 2001. Spectroscopic determination of wheat water status using 1650–1850 nm spectral absorption features. International Journal of Remote Sensing **22**, 2329–2338.

Tompkins, S., Mustard, J. F., Pieters, C. M. and Forsyth, D. W. 1997. Optimization of endmembers for spectral mixture analysis. Remote Sensing of Environment **59**, 472–489.

Whiting, M. L. and Ustin, S. L. 2001. Correlating AVIRIS imagery to field sampling and spectrometer measurements for inorganic soil carbon. In: *Summaries of the 10th JPL Airborne Earth Science Workshop*, edited by R. O. Green (Jet Propulsion Laboratory, Pasadena, CA, USA), pp. 455–461.